Feasibility study of using high-frequency ultrasonic Nakagami imaging for characterizing the cataract lens *in vitro*

Feasibility study of using high-frequency ultrasonic Nakagami imaging for characterizing the cataract lens *in vitro*

Po-Hsiang Tsui[1], Chih-Chung Huang[2,3], Chien-Cheng Chang[1,4], Shyh-Hau Wang[3] and K Kirk Shung[2]

[1] Division of Mechanics, Research Center for Applied Sciences, Academia Sinica, Taipei 11529, Taiwan, Republic of China
[2] NIH Resource on Medical Ultrasonic Transducer Technology, Department of Biomedical Engineering, University of Southern California, 1042 Downey Way, DRB 132, Los Angeles, CA 90089-1111, USA
[3] Department of Biomedical Engineering, Chung Yuan Christian University, Chung Li, 32023, Taiwan, Republic of China
[4] Institute of Applied Mechanics, National Taiwan University, Taipei 10617, Taiwan, Republic of China

E-mail: j648816n@ms23.hinet.net (Chih-Chung Huang) and mechang@gate.sinica.edu.tw (Chien-Cheng Chang)

Abstract

A cataract is a clouding of the crystalline lens that reduces the amount of incoming light and impairs visual perception. Phacoemulsification is the most common surgical method for treating advanced cataracts, and determining the optimal phacoemulsification energy is dependent on measuring the hardness of the lens. This study explored the feasibility of using an ultrasonic parametric image based on the Nakagami distribution to quantify the lens hardness. Young's modulus was measured in porcine lenses in which cataracts had been artificially induced. High-frequency ultrasound at 35 MHz was used to obtain the B-mode and Nakagami images of the cataract lenses. The averaged integrated backscatter and Nakagami parameters were also estimated in the region of interest. The experimental results show that the conventional B-scan and integrated backscatter are inadequate for quantifying the lens hardness, whereas Nakagami imaging allows different degrees of lens hardening to be distinguished both globally and locally based on the concentration of fiber coemption therein.

(Some figures in this article are in colour only in the electronic version)

1. Introduction

A cataract is a clouding of the normally transparent crystalline lens of the eye due to factors such as ageing, lens damage and heredity. The formation of a cataract can be treated as a process of lens fibrosis, whereby both protein aggregation and fiber coemption occur inside the lens (Tabandeh *et al* 2000, Kanski 2006). The lens fibrosis not only results in blurred vision but also increases the hardness of the lens. The initial stage of cataract formation can generally be mitigated using a medical eyewash. However, phacoemulsification is typically applied to advanced cataracts to replace the turbid lens of the patient with an artificial one so as to recover the vision. The lens hardness significantly influences the optimal ultrasonic energy in phacoemulsification, where optimizing the energy improves the efficiency of the surgery and reduces the injury to the lens capsule and corneal endothelium. Consequently, the hardness of the lens should be evaluated before performing phacoemulsification surgery.

Several ultrasound-based methods have been explored for measuring the hardness of the cataract lenses (Sugata *et al* 1992, Tabandeh *et al* 2000, Paunksnis *et al* 2003, Raitelaitienė *et al* 2004, Kurapkienė *et al* 2005, Huang *et al* 2007a, 2007b). Typically, this involves measuring the two echo signals returned from the anterior and posterior interfaces of the lens following stimulation by a single-element ultrasonic transducer positioned outside the eyeball. The sound velocity and attenuation are then estimated from differences in the times of flight of the two echoes and the power spectra of the echoes, respectively. The above studies have demonstrated that both the ultrasonic attenuation and sound velocity tend to increase with the hardness of the cataract lens.

High-frequency ultrasound is also used to locally characterize cataract formation, since a high-frequency ultrasonic B-mode image clearly displays lens structures. Also, the ultrasonographic appearance of the cataract lens differs from that of the normal lens, since optical opacities produce acoustic inhomogeneity, with the cataract area exhibiting high echogenicity (Coleman *et al* 2006). However, the brightness of the ultrasonic B-scan varies with user experience and the system settings, such as the gain, dynamic range and other signal/image processing settings. This results in the B-scan providing only a qualitative description of the cataract lens, limiting the ability to quantify the properties of the cataract lens from the hardness information.

To better characterize the cataract lens, we may further image the cataract lens by ultrasound parameters to reflect the properties of scatterers in the lens. Among all possibilities, the recently proposed ultrasonic parametric imaging based on the Nakagami parameter has a great potential in scatterer analysis (Tsui and Chang 2007). The Nakagami parameter is a shape parameter of the Nakagami statistical distribution that determines the statistical distribution of the ultrasonic backscattered envelope (Hampshire *et al* 1988, Zimmer *et al* 1996, Shankar 2000, 2004, Wachowiak *et al* 2002, Shankar *et al* 2003, Nadarajah 2007). The probability density function $f(r)$ of the ultrasonic backscattered envelope R under the Nakagami statistical model is given by

$$f(r) = \frac{2m^m r^{2m-1}}{\Gamma(m)\Omega^m} \exp\left(-\frac{m}{\Omega}r^2\right) U(r),$$ (1)

where $\Gamma(\cdot)$ and $U(\cdot)$ are the gamma function and the unit step function, respectively. If $E(\cdot)$ denotes the statistical mean, the scaling parameter Ω and the Nakagami parameter m associated with the Nakagami distribution can be respectively obtained from

$$\Omega = E(R^2)$$ (2)
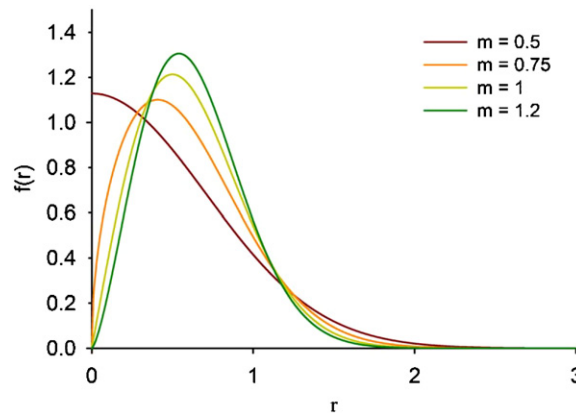
Figure 1. Nakagami distributions for different Nakagami parameters.

and

$$m = \frac{[E(R^2)]^2}{E[R^2 - E(R^2)]^2}.$$ (3)

The statistics of the backscattered envelope changes from a pre-Rayleigh distribution to a Rayleigh distribution as m varies from 0 to 1, and is a post-Rayleigh distribution when m is larger than 1, as shown in figure 1. In other words, the Nakagami distribution can be treated as a general model to describe all the backscattered statistics encountered in medical ultrasound: pre-Rayleigh, Rayleigh and post-Rayleigh distributions. Because the statistics of the backscattered echoes vary with the scatterer concentration (Shankar 2000, Tsui and Wang 2004), the Nakagami image can be used to differentiate the scatterer concentrations in a tissue (Tsui and Chang 2007).

This study explored the feasibility of using the Nakagami image to characterize the cataract lens. We measured Young's modulus in cataracts at different stages that were artificially induced in porcine lenses *in vitro*. The samples were scanned to obtain the B-mode and Nakagami images, and both the averaged integrated backscatter and the Nakagami parameters in the regions of interest were compared with Young's modulus to evaluate the performance of the Nakagami image in quantifying the lens hardness. Here, we also comment on the possible roles of the Nakagami image in cataract diagnosis and treatment.

2. Materials and methods

2.1. Lens sample

Five porcine eyes collected from a local slaughterhouse were used as experimental samples. A surgical knife was used to separate the lenses from the eyes. The lens was then washed carefully with a saline buffer solution to clean the iris remnants and adhering vitreous. The thickness and weight of the lenses were approximately 7.46 ± 0.21 (mean $\pm$ SD) mm and 0.48 ± 0.009 g, respectively. To induce the cataract, the lenses were immersed in a mixture solution of ethanol, 2-propanol and formalin at a ratio of 3:3:4. With increasing immersion time, the lens hardness increases accordingly (Sugiura *et al* 1999). The hardness of the cataract lens was evaluated by measuring Young's modulus using a commercial mechanical device (ElectroForce 3100 Test Instrument, Bose Corporation, Minnesota). First of all, the
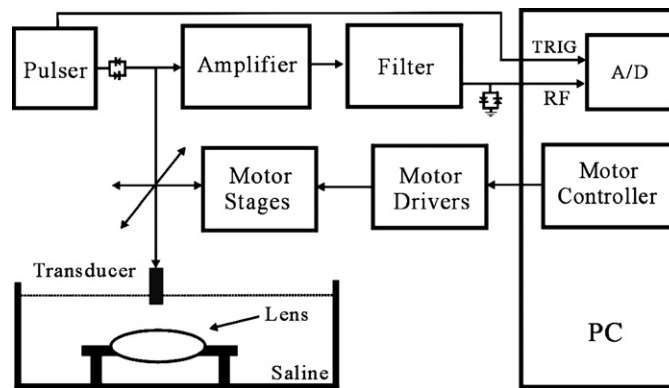
Figure 2. Experimental setup.

Table 1. Characteristics of the ultrasonic transducer.

Piezoelectric material	LiNbO$_3$
Center frequency	35 MHz
F-number	2.6
Focal length	12 mm
Diameter	4.6 mm
Pulselength	77 μm

lens placed on a flat holder was compressed by a circular metal disc, which is driven by a linear motor. Then, the compression force and resulting deformation of the lens were measured using the built-in sensors in the device. The strain rate of the measurement system is 0.02 s^{-1}. The relationship between the stress and strain was calculated with the strain defined as the ratio of the total deformation to the initial thickness. Young's modulus for each specimen at the immersion times of 40, 80, 120 and 160 min was computed from the slope of the stress–strain curve.

2.2. Experimental setup

The experimental setup is shown in figure 2. Prior to measurements, the lens samples were placed on a rectangular polyurethane holder. The distance between the transducer and capsule was about 11 mm. An ultrasonic transducer (NIH Ultrasonic Transducer Resource Center, USC, CA) with a central frequency of 35 MHz was used. The characteristics and pulse-echo tests of the transducer are listed in table 1 and shown in figure 3, respectively. Both the transducer and the lens samples were immersed in a saline buffer solution with a room temperature of about 25.0 °C. The transducer movement was controlled using the motor stage and accessory controller (Parker Hannifin Corp., Cleveland, OH). An ultrasonic pulser (AVB2-TB-C, Avtech Electrosystems Ltd, Ottawa, Ontario, Canada) was used to drive the transducer through an expander (Matec Instruments Company, Northborough, MA) and a T-junction. The radio-frequency (RF) ultrasound signals received from the lens were subsequently amplified by a low-noise amplifier (Miteq 1166, Miteq Inc., Hauppauge, NY), filtered by a band-pass filter (Model BIF-50, Mini-Circuits, Brooklyn, NY) and digitalized using a 14 bit analog-to-digital converter (ADC) (CS14200, Gage Applied Technologies, Inc., Lachine, QC, Canada) at a sampling rate of 200 MHz. Note that an electronic limiter (Matec Instruments Company,
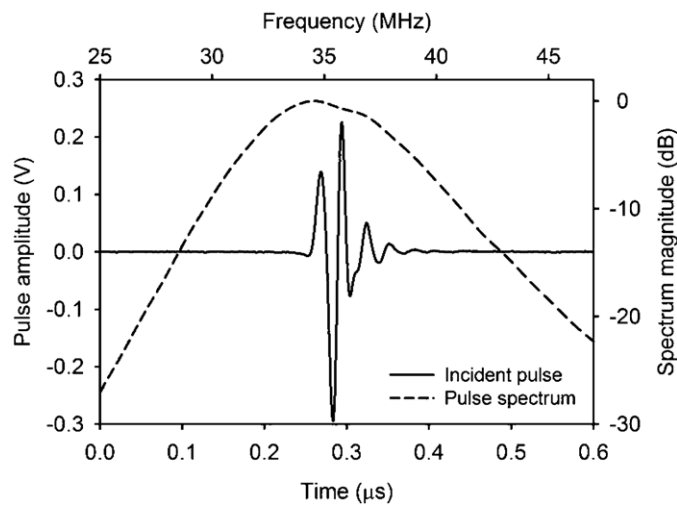
Figure 3. Pulse-echo waveform and frequency spectrum of the transducer.

Northborough, MA) was in front of ADC for protection purposes. For each lens at the immersion times of 40, 80, 120 and 160 min, the image scanning was performed to acquire a total of 1000 A-lines of backscattered signals. The distance between each scan-line is 12 μm. Each scan-line was then demodulated to obtain the envelope image of the lens. The B-mode image is displayed based on the log-compressed envelope image with a dynamic range of 40 dB. The typical B-mode images of a normal and a cataract lens are shown in figures 4(a) and (b), respectively.

2.3. Nakagami image formation

The procedure of Nakagami imaging refers to our previous study (Tsui and Chang 2007). Here, we briefly review this procedure as follows. The Nakagami image is based on the Nakagami parameter map, which is constructed using a square sliding window to process the envelope image (no log-compression). This mainly contains two steps:

(1) A square window within the lens envelope image is used to collect the local backscattered envelopes for estimating the local Nakagami parameter m_w. The parameter m_w is assigned as the new pixel located in the center of the window.
(2) Let the window move throughout the whole envelope image in steps of one pixel, and repeat step 1. Thus, the Nakagami image of the cataract lens can be constructed using the map of the parameter m_w.

Note that the window size determines the resolution of the Nakagami image. As the window size decreases, the resolution of the Nakagami image gets better. However, the small window has fewer envelope data points, leading to an unstable estimation of the parameter m_w. Therefore, prior to the construction of the Nakagami image, the optimal size of the window that can simultaneously satisfy both the stable estimation of m_w and an acceptable resolution of the Nakagami image needed to be determined. The steps to determine the appropriate window size are

(1) A reference phantom with a homogeneous medium is scanned to obtain its envelope image. Each envelope signal of the image scan-line is used to calculate the Nakagami
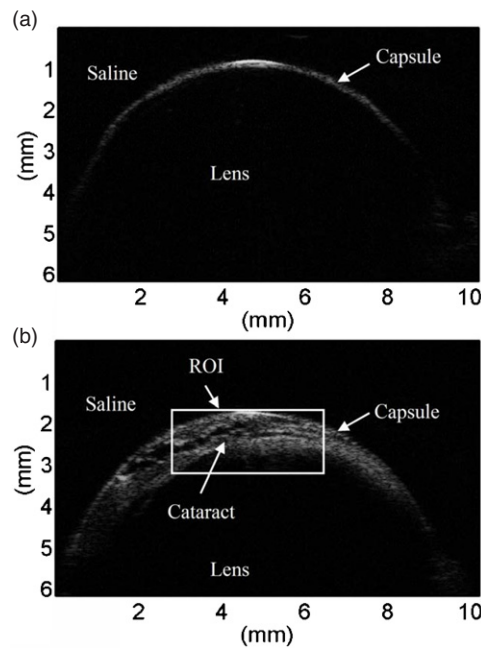
Figure 4. B-mode images of a normal (a) and a cataract lens (b).

parameter m. The average Nakagami parameter $\bar{m}$ is calculated by averaging all m parameters. Under the condition that the length of the envelope signal is long enough to satisfy the stable estimation of m, $\bar{m}$ can be treated as an indicator of the global backscattered statistics of the scanning region.

(2) Each m_w in the scanning region and their average value $\bar{m}_w$ are subsequently estimated using different increasing sizes of the sliding window. Assuming that the window size is large enough (but no too large) to satisfy the stable estimation of the parameter m_w, the result of $\bar{m}_w$ should approach that of $\bar{m}$ to reflect the identical global backscattered statistics. Consequently, the optimal window size is determined once $\bar{m}_w = \bar{m}$.

Based on the conclusion in our previous study (Tsui and Chang 2007), the size of the sliding window used to construct the Nakagami image is the square with the length of a side equal to three times the pulselength of incident ultrasound. For this reason, we constructed the Nakagami images of the lenses using a square window with a size of 231 μm $\times$ 231 μm. To clearly reveal the information of the Nakagami image, the pseudocolor was applied to display the Nakagami parameter map. The parameters m_w smaller than 1 were assigned the blue shades varying from deep to shallow with the increasing parameter value, representing various pre-Rayleigh statistics of the backscattered envelope. When m_w equaled 1, the shade was white to express the Rayleigh distribution, and those larger than 1 were assigned the shades of progressive red color in accordance with the increasing parameter value, indicating the incremental degree of the post-Rayleigh distributions in the backscattered statistics.

2.4. Parameters analysis

After forming the B-mode and Nakagami images of the lens, we further calculated the averaged integrated backscatter (IB, denoted by $\overline{\text{IB}}$) and $\bar{m}_w$ of the region of interest (ROI)
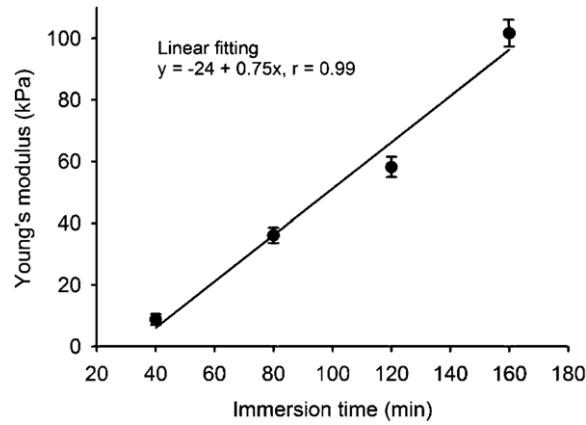
Figure 5. Average Young's modulus as a function of the immersion time.

for comparisons with Young's modulus. The ROI consisted of 300 scan-lines and had a range of 3.6 mm × 1.4 mm, as shown in figure 4(b). IB is defined as the frequency average of the backscattering transfer function of a volume of tissue over the bandwidth of the transducer normalized relative to that from a flat reflector, as given by (O'Donnell *et al* 1979, Vlad *et al* 2005)

$$\text{IB} = \frac{1}{f_2 - f_1} \sum_{f_1}^{f_2} \frac{|S_r(f)|^2}{|S_{\text{ref}}(f)|^2} \tag{4}$$

where $S_r(f)$ and $S_{\text{ref}}(f)$ are Fourier-transform-based power spectra of the RF signals returned from the tissues and the quartz flat reflector in the distilled water, respectively, and f_1 and f_2 denote the lower and upper frequencies of the -6 dB bandwidth of the spectrum. Therefore, $\overline{\text{IB}}$ is obtained by averaging all IB estimated from each A-line in the ROI, and $\bar{m}_\text{w}$ is calculated by averaging all m_w in the ROI.

3. Results and discussion

Figure 5 shows that the measured Young's modulus of the lens increased from approximately 8 to 100 kPa as the immersion time increased from 40 to 160 min (correlation coefficient $r = 0.99$), corresponding to a rate of increase of 0.77 kPa min^{-1}.

Figure 6(a) shows the B-mode image of the normal lens. Figures 6(b)–(e) show the B-mode images of the cataract lens for different immersion times at 40, 80, 120 and 160 min, respectively, which clearly show the internal structures and cataract areas containing fiber coemption. It was found that the image brightness of the lens front interface (i.e., capsule) increased with increasing the immersion time, representing that the echo reflection at the capsule increases with the lens hardness. However, the variation of the brightness in the B-scan appears weak and may depend on the system settings (e.g., dynamic range and system gain) and user experiences. Therefore, the B-mode image may be limited when used to detect the hardness of the lens tissue. To further check this point, we calculated $\overline{\text{IB}}$ in the ROI as a function of the immersion time, as shown in figure 7, to quantify how the intensities of the ultrasonic echoes differed with the stage of the cataract. The linear fitting shows that $\overline{\text{IB}}$ increased from -168 to -164 dB with increasing the immersion time from 40 to 160 min
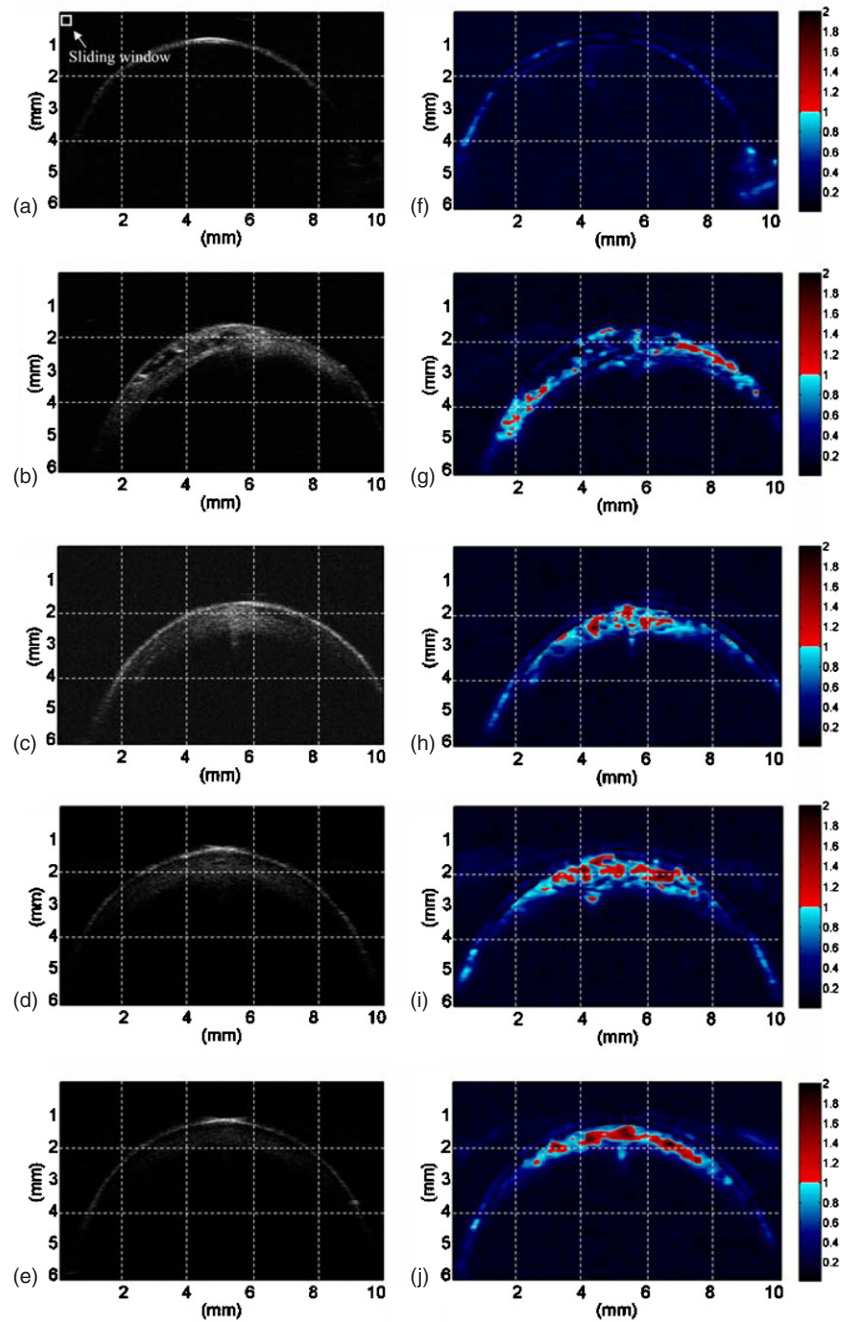
Figure 6. Representative B-mode images ((a)–(e)) and Nakagami images ((f)–(j)) of the porcine lens at different stages of cataract formation.

$(r = 0.31)$. This corresponds to a rate of increase at 0.033 dB min^{-1}. $\overline{\text{IB}}$ did not change significantly and had a large variance while the lens was immersed in the mixture solution, indicating that the backscattering intensity may be weak to differentiate the hardness of the
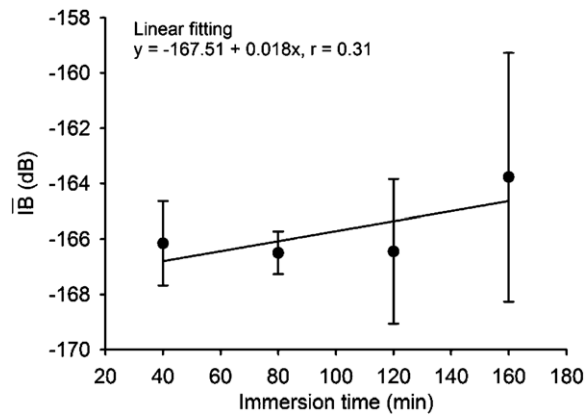
Figure 7. Average integrated backscatter as a function of the immersion time.
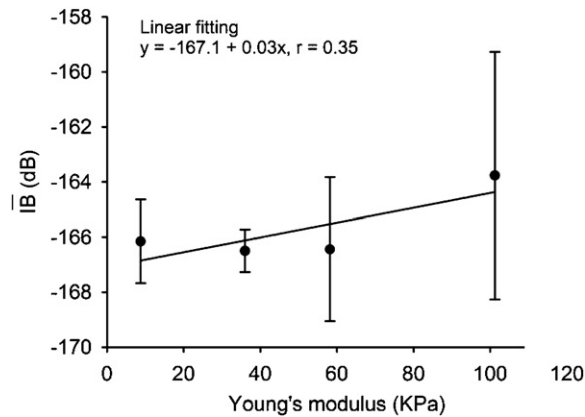

Figure 8. Average integrated backscatter as a function of Young's modulus.

cataract lens. This can be further demonstrated by comparing the integrated backscatter and Young's modulus, as shown in figure 8. This result shows that $\overline{\text{IB}}$ increased from -168 to -164 dB as Young's modulus increased from 8 to 100 kPa. This corresponds to a rate of increase at 0.043 dB kPa^{-1}. As a result, the correlation between the integrated backscatter and Young's modulus was not very good ($r = 0.35$). The reason may be due to the echogenicity being largely unaffected by protein aggregation and fiber coemption, resulting in negligible effects on the amplitudes of the backscattered signals.

Figures 6(f)–(j) show the Nakagami images corresponding to the B-mode images in figures 6(a)–(e). Most dark shadings in the Nakagami images corresponded to the background (saline buffer solution) and the transparent portions of the lens. This is because these regions essentially have few scatterers inside, and the backscattered statistics tends to be pre-Rayleigh distributions. Note that blue shading was more evident in the cataract regions in the Nakagami images for shorter immersion times, which indicates that the statistics of the local ultrasonic backscattered envelope were dominated by a pre-Rayleigh distribution ($m_w < 1$). Increasing the immersion time resulted in more red shading in the ROIs of the Nakagami images,
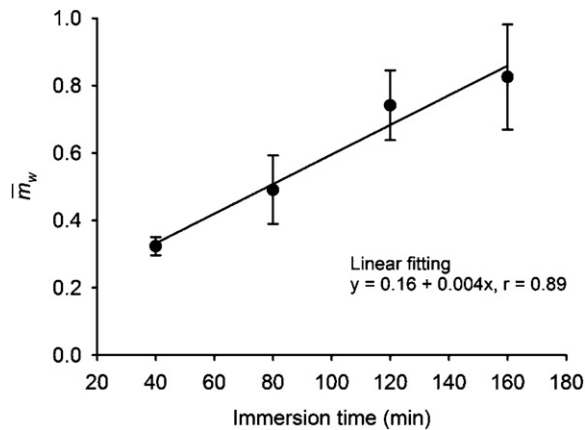
Figure 9. Average local Nakagami parameter as a function of the immersion time.
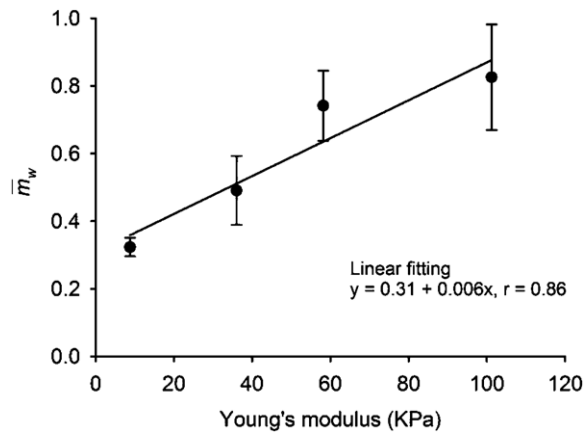
Figure 10. Average local Nakagami parameter as a function of Young's modulus.

indicating that the primary statistical distribution of the local envelope followed post-Rayleigh statistics ($m_w > 1$). The average value of m_w in the ROI, $\bar{m}_w$, is plotted as a function of the immersion time in figure 9, which shows that $\bar{m}_w$ increased from about 0.3 to 0.8 as the immersion time increased from 40 to 160 min ($r = 0.89$), corresponding to a rate of increase of 0.004 min^{-1}. This indicates that the global statistics of the backscattered envelope in the ROI varied from a pre-Rayleigh distribution to roughly a Rayleigh distribution as the immersion time increased. Figure 10 plots $\bar{m}_w$ versus Young's modulus of the cataract lens for different immersion times and shows that $\bar{m}_w$ increased from 0.3 to 0.8 as Young's modulus increased from 8 to 100 kPa, corresponding to a rate of increase of 0.005 kPa^{-1} ($r = 0.86$). The high correlation coefficient indicates that the Nakagami image is suitable for locally distinguishing variations in the hardness of the cataract lens. Moreover, the overall lens hardness can be determined by averaging all the m_w values in the ROI in the Nakagami image.

It must be noted that the blue and red shadings in the Nakagami images were caused by the interior variation of the structures in the lens instead of the lens front edge (capsule). This is because the thickness of the capsule is around 0.2 mm and the sliding window size

is 0.23 mm × 0.23 mm. It means that the capsule thickness is smaller or comparable to the resolution of the Nakagami parametric image. Consequently, when the sliding window moves onto the capsule, the window not only covers the signals from the front interface but also contains those from partial background or lens. Because the front interface contributes stronger echoes than the background and lens do, the statistical distribution of the backscattered envelopes acquired by the window would tend to be pre-Rayleigh statistics, rendering the Nakagami parameter small and that the capsule has dark blue shadings in the Nakagami image. This may be called the subresolvable effect of Nakagami imaging. In other words, if the sliding window does not include the capsule, the Nakagami image can more accurately reflect the change in the backscattered statistics from pre-Rayleigh to post-Rayleigh due to the lens hardening.

The mechanism underlying how Nakagami techniques (i.e., m_w estimation and the corresponding mapping) could be used in medical ultrasound to differentiate the lens hardness is not yet clear, but possible explanations are given below. The protein aggregation and fiber coemption that occur in the lens in the presence of a cataract increase the lens hardness. If the lens tissue is modeled as a collection of scatterers, cataract formation involves changing the arrangement and concentration of these scatterers corresponding to protein and fibers, and accordingly detecting the variation in the scatterer concentration of the lens is integral to determining the hardness of the cataract lens. Although the term 'scatterer concentration' is a theoretical concept in real biological tissues, it is still possible to indirectly estimate the scatterer concentrations in tissues by analyzing the statistical distribution of the backscattered envelopes. This is because the ultrasonic backscattered statistics varies with the scatterer concentration, as verified by computer simulations and phantom experiments (Shankar 2000, Tsui and Wang 2004). It is worthwhile to refer to some literatures for understanding the relationship between the backscattered statistics and the scatterer arrangements. The envelope statistics of the Rayleigh distribution occurs when the resolution cell of the ultrasonic transducer contains a large number of randomly distributed scatterers (Burckhardt 1978). If the resolution cell contains the scatterers that have randomly varying scattering cross sections with a comparatively high degree of variance, the envelope statistics are pre-Rayleigh distributions, and as the resolution cell contains the periodically located scatterers in addition to the randomly distributed scatterers, the envelope statistics are post-Rayleigh distributions (Shankar 2000, Shankar *et al* 2001). Consequently, for a normal lens, we can see that the statistical distribution of the backscattered envelope is extremely pre-Rayleigh statistics ($m_w \ll 1$) (figure 6(f)). In other words, the lens has nearly no scatterer (i.e., no lens fibrosis). Figures 6(g) and 10 indicate that the global and local backscattered statistics in the early stage of cataract formation (i.e., with a short immersion time) have a pre-Rayleigh distribution ($\bar{m}_w < 1$ in the ROI, with $m_w < 1$ mostly). Therefore, the scatterer concentration can be considered to be comparatively low in the cataract region of the lens, which corresponds to little protein aggregation and fiber coemption being present in the initial stage of cataract formation. For cataracts at later stages, the global backscattered statistics of the ROI gradually approaches a Rayleigh distribution ($\bar{m}_w \approx 1$ in the ROI) (figure 10), with the local statistics of the ultrasonic envelopes represented by different degrees of a post-Rayleigh distribution ($m_w > 1$ mostly) (figures 6(h)–(j)). The long immersion times required to form a cataract lens strongly induce protein aggregation and fiber coemption, causing the scatterer concentration to increase.

4. Concluding remarks

In this study, we explored the usefulness of Nakagami imaging in characterizing cataract lenses by investigating porcine eyes using 35 MHz high-frequency ultrasound. The results

have shown that the B-mode image clearly reveals the structures of the cataract lens, but it is difficult to use this and the associated IB to determine the lens hardness. In contrast, Nakagami imaging can be used to distinguish both global and local variations in the lens hardness. This is because the scatterer concentration of the fiber coemption—which is mainly responsible for the increase in the lens hardness during cataract formation—can be quantified using the Nakagami technique to analyze the statistical distribution of the ultrasonic backscattered echoes. The presented experimental findings show that Nakagami imaging has great potential to complement conventional B-scans in simultaneously evaluating the structure and elastic properties of the lens. This information may help in determining the optimal energy to apply during phacoemulsification. Nevertheless, experimental and clinical validations must be carried out before the Nakagami image can be used as a reliable clinical tool in ophthalmology applications.

Acknowledgments

References

Burckhardt C B 1978 Speckle in ultrasound B-mode scans *IEEE Trans. Sonics Ultrason.* **25** 1–6

Coleman D J, Silverman R H, Lizzi F L and Rondeau M J 2006 *Ultrasonography of the Eye and Orbit* (Philadelphia, PA: Lippincott Williams & Wilkins)

Hampshire J B I, Strohbehn J W, McDaniel M D, Waugh J L and James D H 1988 Probability density of myocardial ultrasonic backscatter *Proc. 14th Ann. Northeast Bioeng. Conf. (March)* pp 305–8

Huang C C, Ameri H, DeBoer C, Rowley A P, Xu X, Sun L, Wang S H, Humayun M S and Shung K K 2007a Evaluation of lens hardness in cataract surgery using high frequency ultrasonic parameters *in vitro Ultrasound Med. Biol.* **33** 1604–16

Huang C C, Zhou Q, Ameri H, Wu D, Sun L, Wang S H, Humayun M S and Shung K K 2007b Determining the acoustic properties of the lens using a high-frequency ultrasonic needle transducer *Ultrasound Med. Biol.* at press

Kanski J J 2006 *Clinical Diagnosis in Ophthalmology* (London: Elsevier)

Kurapkienė S, Raitelaitienė R, Paunksnis A, Lukoševičius A, Burnovas S, Paunksnienė M, Svaldenienė E and Babrauskienė V 2005 The relationship of ultrasonic and mechanical properties of human nuclear cataract: a pilot study *Ultragarsas.* **1** 39–43

Nadarajah S 2007 Statistical distributions of potential interest in ultrasound speckle analysis *Phys. Med. Biol.* **52** N213–27

O'Donnell M, Bauwens D, Mimbs J W and Miller J G 1979 Broadband integrated backscatter: an approach to spatially localized tissue characterization *in vivo IEEE Ultrason. Symp.* **1** 175–8

Paunksnis A, Kurapkienė S, Mačiulis A, Raitelaitienė R, Jurkonis R and Lukoševičius A 2003 Estimation of ultrasound attenuation coefficient of human diabetic cataract *Ultragarsas.* **1** 37–40

Raitelaitienė R, Kurapkienė S, Mačiulis A and Paunksnis A 2004 The influence of age related changes to ultrasound attenuation of human eye lens *Ultragarsas.* **2** 55–9

Shankar P M 2000 A general statistical model for ultrasonic backscattering from tissues *IEEE Trans. Ultrason. Ferroelec. Freq. Contr.* **47** 727–36

Shankar P M 2004 The use of the compound probability density function in ultrasonic tissue characterization *Phys. Med. Biol.* **49** 1007–15

Shankar P M, Dumane V A, George T, Piccoli C W, Reid J M, Forsberg F and Goldberg B B 2003 Classification of breast masses in ultrasonic B scans using Nakagami and K distributions *Phys. Med. Biol.* **14** 2229–40

Shankar P M, Dumane V A, Reid J M, Genis V, Forsberg F, Piccoli C W and Goldberg B B 2001 Classification of ultrasonic B-mode images of breast masses using Nakagami distribution *IEEE Trans. Ultrason. Ferroelec. Freq. Contr.* **48** 569–80

Sugata Y, Murakami K, Ito M, Shiina T and Yamamoto Y 1992 An application of ultrasonic tissue characterization to the diagnosis of cataract *Acta Ophthalmol. Suppl.* **204** 35–9

Sugiura T, Kurosaks D, Uezuki Y, Eguchi S, Obata H and Takahashi T 1999 Creating cataract in pig eye *J. Catatact Refract. Surg.* **25** 615–21

Tabandeh H, Wilkins M, Thompson G, Nassiri D and Karim A 2000 Hardness and ultrasonic characteristics of human crystalline lens *J. Catatact Refract. Surg.* **26** 838–41

Tsui P H and Chang C C 2007 Imaging local scatterer concentrations by the Nakagami statistical model *Ultrasound Med. Biol.* **33** 608–19

Tsui P H and Wang S H 2004 The effect of transducer characteristics on the estimation of Nakagami parameter as a function of scatterer concentration *Ultrasound Med. Biol.* **30** 1345–53

Vlad R M, Czarnota G J, Giles A, Sherar M D, Hunt J W and Kolios M C 2005 High-frequency ultrasound for monitoring changes in liver tissue during preservation *Phys. Med. Biol.* **50** 197–213

Wachowiak M P, Smolikova R, Tourassi G D and Elmaghraby A S 2002 General ultrasound speckle models in determining scatterer density *Proc. SPIE* **4687** 285–95

Zimmer Y, Akselrod S and Tepper R 1996 The distribution of the local entropy in ultrasound images *Ultrasound Med. Biol.* **22** 431–9